Parameterization of shortwave ice cloud optical properties for various particle habits

Jeffrey R. Key,[1] Ping Yang,[2] Bryan A. Baum,[3,4] and Shaima L. Nasiri[5]

Received 17 April 2001; revised 27 November 2001; accepted 1 December 2001; published 12 July 2002.

[1] The relative importance of ice clouds in the climate system is highly uncertain. Measurements of their microphysical properties are sparse, especially given their complex structure and large variability in particle size, shape, and density. To better understand the role of ice clouds in the climate system, parameterizations of their radiative properties are needed. The shortwave bulk optical properties of seven ice particle shapes, or "habits," are parameterized as a function of the effective "radius" and ice water content by integrating the scattering properties over 30 in situ size distributions. The particle habits are solid and hollow hexagonal columns, hexagonal plates, two- and three-dimensional bullet rosettes, aggregates of columns, and dendrites. Parameterizations of the volume extinction coefficient, single-scattering albedo, and the asymmetry parameter are presented for 6, 24, and 56 band shortwave schemes from 0.2 to 5.0 μm. Applications to downwelling flux and upwelling radiance calculations indicate that differences in fluxes for various habits can be more than 15%, and differences in retrievals of cloud optical depth from satellite visible reflectances can be more than 50%. *INDEX TERMS:* 3359 Meteorology and Atmospheric Dynamics: Radiative processes; 0360 Atmospheric Composition and Structure: Transmission and scattering of radiation; 3360 Meteorology and Atmospheric Dynamics: Remote sensing; *KEYWORDS:* clouds, optical properties, radiative transfer, ice particles

1. Introduction

[2] Ice clouds occur globally and at all times of the year, regularly covering up to 40% of the earth [*Wylie et al.*, 1994]. They are vertically distributed from the upper troposphere and lower stratosphere in the tropics to the lower troposphere in the polar regions during the winter. They strongly influence weather and climate processes on all scales through their effects on the radiative budget. Cirrus clouds have been identified as one of the most uncertain components in regulating the Earth's climate and its variability [*Liou*, 1986, 1992; *Stephens et al.*, 1990]. The relative importance of the cloud shortwave albedo effect and the cloud thermal "greenhouse" effect is unknown, so it is not clear whether cirrus clouds heat or cool the Earth-atmosphere system. To better understand the role of ice clouds in the climate system, parameterizations of their radiative properties for climate models and satellite simulations are needed.

[3] Ice cloud radiative properties depend on the ice crystal optical properties, which in turn depend on the microphysical properties. The microphysical properties of interest are the particle shape, particle size distribution, and the ice water content. Ice clouds with large crystals are almost exclusively composed of nonspherical ice crystals of various shapes and sizes. The geometric optics method of ray tracing has been used to determine the single-scattering properties of nonspherical ice crystals. *Takano and Liou* [1989] presented an empirical equation relating the single-scattering albedo of hexagonal crystals to the aspect ratio and absorption coefficient. *Ebert and Curry* [1992] extended the work of *Takano and Liou* [1989] in the development of a parameterization of ice cloud optical properties for five shortwave and five longwave bands. The single-scattering albedo, asymmetry parameter, mass extinction coefficient, and mass absorption coefficient were parameterized as a function of the particle effective radius of hexagonal crystals and the water path. *Fu and Liou* [1993] used an exact spheroid solution for small particles and ray tracing for larger hexagonal crystals in the parameterization of ice cloud optical properties in six shortwave and 12 longwave bands. *Fu* [1996] used the geometric-optics-integration-equation technique [*Yang and Liou*, 1996b] (hereinafter referred to as GOM2) to compute the single-scattering properties of columns and plates. *Grenfell and Warren* [1999] took a different approach, modeling the optical properties of ice clouds by representing each nonspherical particle by a collection of independent spheres, each having the same volume-to-surface ratio as the nonspherical particle.

[1]Office of Research and Applications, National Environmental Satellite, Data, and Information Service, National Oceanic and Atmospheric Administration, Madision, Wisconsin, USA.
[2]Department of Atmospheric Sciences, Texas A&M University, College Station, Texas, USA.
[3]NASA Langley Research Center, Hampton, Virginia, USA.
[4]Also at Cooperative Institute for Meteorological Satellite Studies, University of Wisconsin, Madison, Wisconsin, USA.
[5]Cooperative Institute for Meteorological Satellite Studies, University of Wisconsin, Madison, Wisconsin, USA.

0148-0227/02/2001JD000742$09.00

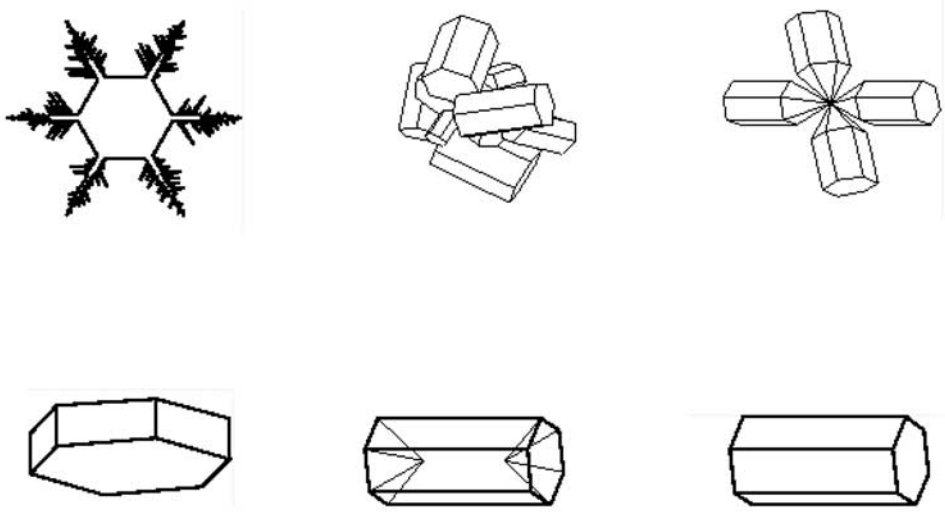

Figure 1. Idealized shapes of the particle habits. Clockwise from top left: dendrite, aggregate, bullet rosette, solid column, hollow column, and plate.

[4] Observations from aircraft two-dimensional cloud (2-D-C) probes and balloon-borne replicators have shown that the majority of particles in ice clouds are bullet rosettes, solid and hollow columns, plates, and aggregates with maximum dimensions ranging from 5 to about 1000 μm [cf. *Heymsfield and Platt*, 1984; *Sassen et al.*, 1995; *Mitchell et al.*, 1996a, 1996b]. The optical properties of such complex crystal shapes differs substantially from those of spheres and hexagonal columns [*Takano and Liou*, 1995; *Iaquinta et al.*, 1995; *Macke et al.*, 1996; *Yang and Liou*, 1998; *Wyser and Yang*, 1998]. Reflection by bullet rosettes and planar polycrystals computed from anomalous diffraction theory (ADT) may be more than twice that of hexagonal columns and plates [*Mitchell et al.*, 1996b].

[5] Recently, *Yang et al.* [2000] (hereinafter referred to as YANG00) computed the scattering and geometric properties of a variety of ice crystal shapes and sizes. They developed a parameterization of the extinction and absorption efficiencies, asymmetry factor, and the phase function truncation factor at discrete wavelengths and particle sizes. In this paper we extend the YANG00 work, parameterizing the shortwave bulk optical properties of seven ice particle shapes, or "habits," by integrating the scattering properties over 30 size distributions. The particle habits are solid and hollow hexagonal columns, hexagonal plates, two- and three-dimensional bullet rosettes, aggregates of columns, and dendrites (Figure 1). Parameterizations of the volume extinction coefficient, single-scattering albedo, and the asymmetry parameter are described for the six shortwave bands of *Fu and Liou* [1993], the 24-band scheme of *Slingo and Schrecker* [1982], and the 56 bands of YANG00, each covering approximately 0.2 to 5.0 μm.

[6] The methodology is presented in section 2. The YANG00 work is briefly described and the optical properties of individual crystals are integrated over size distributions for the various particle habits. The optical property parameterizations are then applied to illustrate the effect of particle shape on downwelling fluxes at the surface and upwelling radiances at the top of the atmosphere.

2. Methodology

[7] The general methodology for the parameterization of ice cloud optical properties is as follows: The scattering properties of individual crystals are integrated over observed size distributions and also integrated over the desired spectral bands. Each size distribution yields a value for ice water content and effective size (the microphysical properties), and the corresponding volume extinction coefficient, single-scattering albedo, and asymmetry parameter (the optical properties). The statistical relationship between the optical properties and the microphysical properties is determined with a nonlinear regression procedure.

2.1. Size Distributions

[8] The 30 particle size distributions used in this study are derived from in situ measurements from both midlatitude and tropical cirrus. Detailed descriptions of their properties are given by *Fu* [1996]. The in situ measurements were derived during field campaigns such as FIRE I and FIRE II (FIRE refers to the First ISCCP (International Satellite Cloud Climatology Project) Regional Experiment) and the Central Equatorial Pacific Experiment (CEPEX). Additional cirrus data are provided by *Heymsfield and Platt* [1984], who presented size distributions typical of warm and cold cirrus clouds, cirrostratus, and cirrus uncinus, as well as distributions that represent midlatitude cirrus for a number of discrete temperature intervals from -20°C to -60°C.

[9] Figure 2 shows three of the 30 size distributions obtained from aircraft measurements. These size distributions have been discretized to 38 size bins. The other size distributions fall within the size and number concentration ranges of these three. The use of these size distributions does not guarantee global applicability, though they do

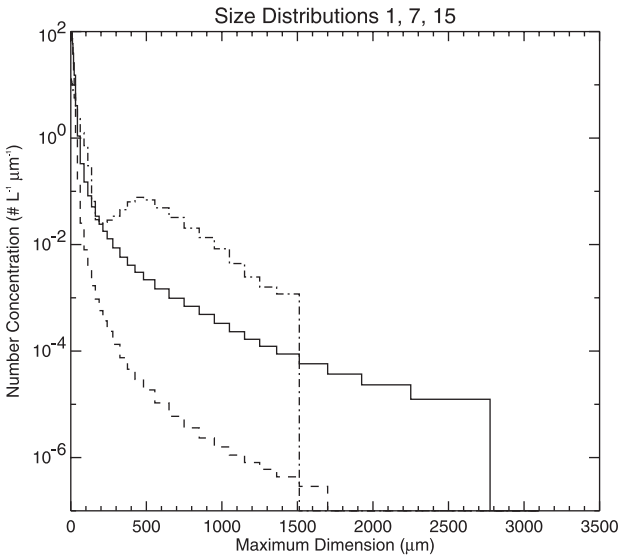

Figure 2. Three of the 30 Fu size distributions obtained from aircraft measurements. The other size distributions fall within the size and number concentration ranges of these three.

cover a wide range of conditions. It is possible, however, that different formation processes will determine the nature of the size distribution and that particular habits have preferred size distribution shapes. At present there is not enough in situ data to determine if such relationships do, in fact, exist.

[10] For each distribution the "effective radius" and ice water content are calculated. The effective radius is half the effective size, defined as

$$R_e = \frac{3}{4}\frac{\sum_{L=L_{min}}^{L_{max}} V(L)n(L)\Delta L}{\sum_{L=L_{min}}^{L_{max}} A(L)n(L)\Delta L} \quad (1)$$

where L is the maximum dimension of an ice crystal, $n(L)$ is the number of particles with maximum dimension L in the size distribution, ΔL is the width of a size bin, and V and A are the volume and total projected area of the particles, respectively. The volume and area are based on the spherical diameter with equivalent volume and the spherical diameter with equivalent projected area as defined by YANG00.

[11] Figure 3 illustrates the relationship between the effective radius and another size metric, the mean maximum "radius," of each size distribution for each habit. The mean maximum radius R_L is half of the mean of the maximum dimensions for a size distribution:

$$R_L = \frac{1}{2}\frac{\sum_{L=L_{min}}^{L_{max}} Ln(L)\Delta L}{\sum_{L=L_{min}}^{L_{max}} n(L)\Delta L} \quad (2)$$

The figure shows that the two size metrics increase together, rapidly at the smaller sizes and less rapidly for large particles. The correlation between them is not strong as a result of the large variability in the size distributions. For example, a mean maximum radius of approximately 40 μm for solid columns corresponds to an effective radius of 40 μm in one distribution but 70 μm in another. Given that the effective radius indirectly accounts for the aspect ratio of the particles and given that it is analogous to the effective radius quantity commonly used with liquid drop size distributions, we consider it to be the more robust of the two size metrics.

[12] The ice water content of the size distribution is

$$WC = \rho_{ice}\sum_{L=L_{min}}^{L_{max}} V(L)n(L)\Delta L \quad (3)$$

where ρ_{ice} is the density of ice, here taken to be 0.9167 g cm^{-3}. The effective radii and ice water contents of each habit for each of the 30 size distributions are shown in Figure 4. Table 1 gives the effective radius and ice water content statistics for each habit over all size distributions. The effective radius of dendrites is significantly smaller than that of the other habits because of the small volume to area ratio.

2.2. Optical Properties

[13] The scattering properties of individual ice crystals and the methods for obtaining them are presented by YANG00 and the references cited therein. The particle habits are solid and hollow hexagonal columns, hexagonal plates, planar and spatial bullet rosettes, rough aggregates, and dendrites. The planar rosettes have four "bullets" arranged on a plane (Figure 1), while the

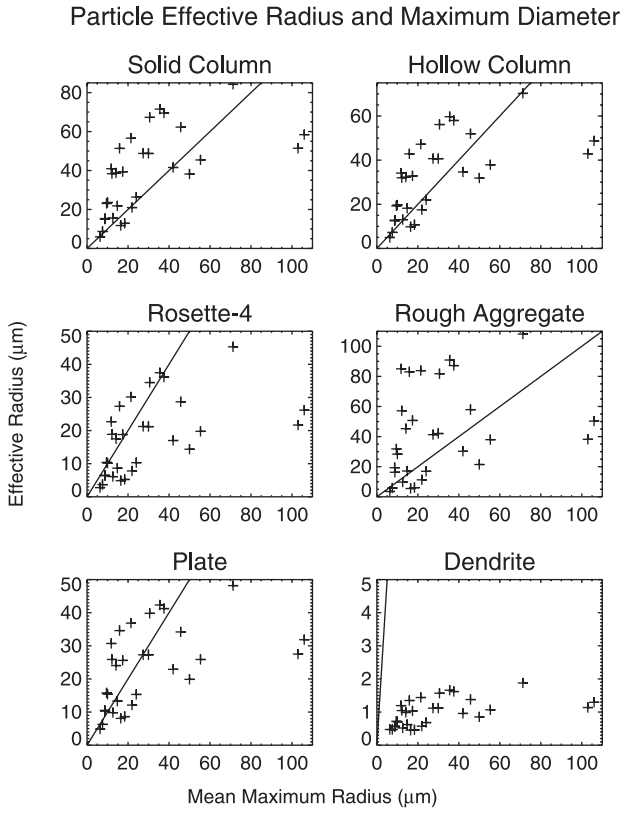

Figure 3. Comparison of the effective radius and the maximum dimension for six of the seven particle habits over the 30 size distributions. The line of one-to-one correspondence is shown. The size metrics of the bullet rosette-6 habit (not shown) are similar to those of the bullet rosette-4 habit. The vertical scale is different for each plot.

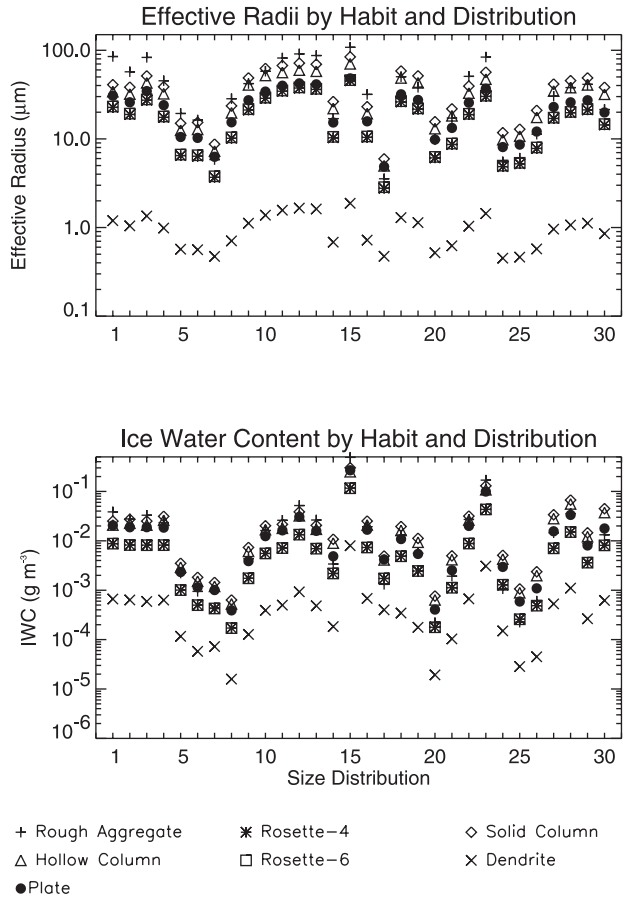

Figure 4. Effective radii and water contents of each habit for each of the 30 size distributions.

spatial rosettes are essentially three-dimensional, with the four bullets of the planar rosettes and two additional bullets extending from the center to either side of the plane. Because the wavelengths involved in the calculation are limited to solar spectrum, an improved geometric optics method (GOM2) is used to derive the single-scattering properties [*Yang and Liou*, 1996a]. In GOM2 the ray-tracing technique is employed to calculate the near field on the particle surface, and the corresponding field in the radiation zone is obtained by mapping the near field to its far-field counterpart. For the computation of extinction and absorption cross sections and the asymmetry factor of the phase function, the GOM2 solutions converge to results given by the finite-difference time domain (FDTD) method [*Yang and Liou*, 1996b] when the size parameter is larger than 15 or 20. In the calculation of single-scattering properties, aspect ratio relationships derived from in situ measurements were used to define the three-dimensional geometry for ice crystals with the given maximum dimensions.

[14] Optical properties for each particle habit are integrated over the size distributions and spectral bands. The volume extinction coefficient for a given band is computed from the extinction efficiency Q_e and projected area provided by YANG00 as

$$\langle \beta_{ext} \rangle = \sum_{L=L_{min}}^{L_{max}} Q_e(L) A(L) n(L) \Delta L \tag{4}$$

In the integration the single-scattering albedo ω and the asymmetry parameter g are weighted by the extinction and scattering cross sections:

$$\langle \omega \rangle = \frac{\sum_{L=L_{min}}^{L_{max}} \omega(L) \sigma_e(L) n(L) \Delta L}{\sum_{L=L_{min}}^{L_{max}} \sigma_e(L) n(L) \Delta L} \tag{5}$$

$$\langle g \rangle = \frac{\sum_{L=L_{min}}^{L_{max}} g(L) \sigma_s(L) n(L) \Delta L}{\sum_{L=L_{min}}^{L_{max}} \sigma_s(L) n(L) \Delta L} \tag{6}$$

where the extinction cross section is $\sigma_e = Q_e A$ and the scattering cross section is $\sigma_s = Q_s A = \omega Q_e A$ with scattering efficiency Q_s. The angle brackets in the above equations denote an average over the distribution, but they will be dropped from subsequent references to β_{ext}, ω, and g. In the integrations over the size distributions the optical properties, volume, and area in the YANG00 database which fall within a size bin are averaged with an inverse distance weighting scheme, where values close to the size bin center receive a higher weight than values farther from the center.

[15] Figure 5 shows the relationship between the optical properties, as defined above, and the effective radius for solid columns. Results are given for four wavelengths across the solar spectrum. Other habits exhibit similar relationships. The overall strength of the relationships

Table 1. Effective Radius and Ice Water Content Statistics for Each Habit Over All Size Distributions

Particle Habit	Min *Re*	Max *Re*	Mean *Re*	SD *Re*	Min IWC	Max IWC	Mean IWC	SD IWC
Agg-rough	3.55	108.10	42.13	30.50	2.20e-04	4.89e-01	3.52e-02	9.13e-02
Bullet-4	2.77	45.30	18.05	11.40	1.71e-04	1.16e-01	9.80e-03	2.17e-02
Column	5.96	84.22	38.46	21.16	6.33e-04	3.00e-01	3.11e-02	5.69e-02
Hollow	4.97	70.24	32.08	17.65	5.28e-04	2.50e-01	2.59e-02	4.75e-02
Bullet-6	2.85	46.01	18.41	11.57	1.71e-04	1.16e-01	9.79e-03	2.16e-02
Den	0.45	1.88	0.98	0.41	1.59e-05	7.98e-03	7.19e-04	1.48e-03
Plate	4.87	48.18	23.21	12.05	3.90e-04	2.68e-01	2.24e-02	5.00e-02

Min, minimum; max, maximum; SD, standard deviation. Effective radius is in microns; ice water content is in g m^{-3}; bullet-4 is the planar bullet rosette; bullet-6" is the spatial rosette. Read 2.20e-04 as 2.20×10^{-4}.

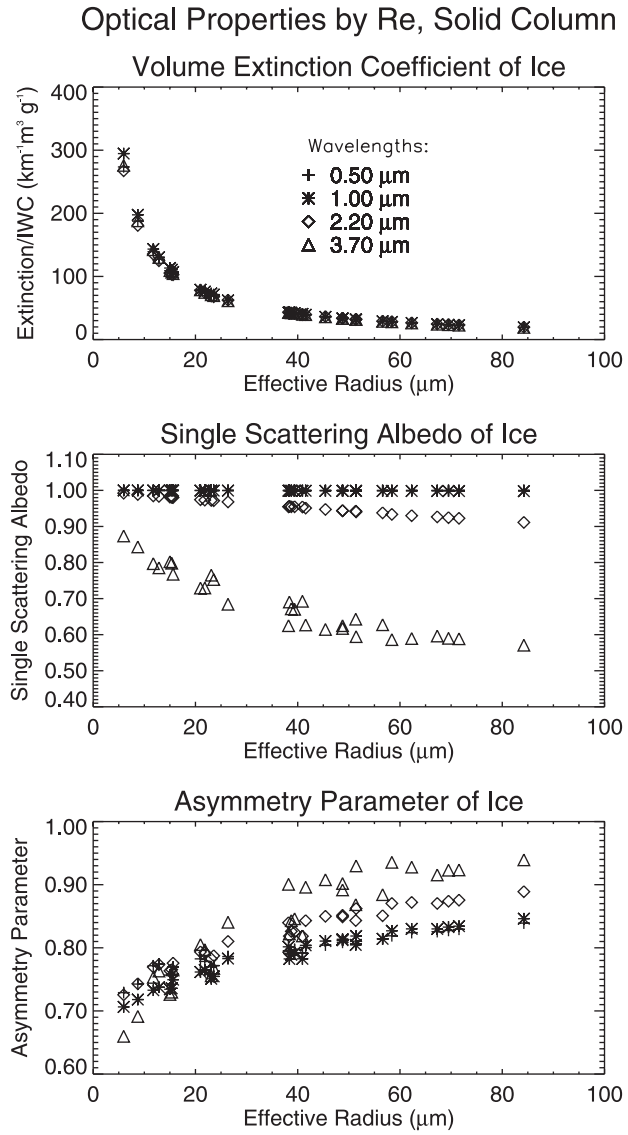

Figure 5. Optical properties of solid columns as a function of effective radius. Each point corresponds to a different size distribution. Results are given for four wavelengths, as indicated in the top plot.

implies that the optical properties can be parameterized as a function of the ice water content (in the case of the extinction coefficient) and the effective radius.

[16] The scattering phase function can be integrated in the same manner as the asymmetry parameter:

$$\langle P(\theta)\rangle = \frac{\sum_{L=L_{min}}^{L_{max}} P(\theta, L)\sigma_s(L)n(L)\Delta L}{\sum_{L=L_{min}}^{L_{max}} \sigma_s(L)n(L)\Delta L} \quad (7)$$

where θ is the scattering angle. Parameterization of the phase function is beyond the scope of this paper. Instead, the integrated phase function for each size distribution is used to determine parameters of the double Henyey-Greenstein function, as discussed in section 2.3.

2.3. Parameterization of Optical Properties

[17] A statistical relationship between the optical and the microphysical properties is formulated as

Table 2. Three Spectral Band Schemes, Specified by Minimum and Maximum Wavelengths

Fu and Liou [1993] 6 bands		*Slingo and Schrecker* [1982] 24 bands		*Yang et al.* [2001] 56 bands	
λ_{min}	λ_{max}	λ_{min}	λ_{max}	λ_{min}	λ_{max}
0.2	0.7	0.28	0.30	0.20	0.25
		0.30	0.33	0.25	0.30
		033	0.36	0.30	0.40
		0.36	0.40	0.40	0.45
		0.40	0.44	0.45	0.50
		0.44	0.48	0.50	0.60
		0.48	0.52	0.60	0.70
		0.52	0.57		
		0.57	0.64		
		0.64	0.69		
0.7	1.3	0.69	0.75	0.70	0.80
		0.75	0.78	0.80	0.90
		0.78	0.87	0.90	1.00
		0.87	1.00	1.00	1.10
		1.00	1.10	1.10	1.20
		1.10	1.19	1.20	1.30
		1.19	1.28		
1.3	1.9	1.28	1.53	1.30	1.40
		1.53	1.64	1.40	1.50
				1.50	1.65
				1.65	1.80
				1.80	1.90
1.9	2.5	1.64	2.13	1.90	1.95
		2.13	2.38	1.95	2.00
				2.00	2.10
				2.10	2.20
				2.20	2.30
				2.30	2.40
2.5	3.5	2.38	2.91	2.40	2.60
		2.91	3.42	2.60	2.70
				2.70	2.80
				2.80	2.83
				2.83	2.85
				2.85	2.88
				2.88	2.90
				2.90	2.92
				2.92	2.95
				2.95	2.97
				2.97	3.00
				3.00	3.03
				3.03	3.05
				3.05	3.08
				3.08	3.10
				3.10	3.12
				3.12	3.15
				3.15	3.17
				3.17	3.20
				3.20	3.25
				3.25	3.30
				3.30	3.40
				3.40	3.50
3.5	4.0	3.42	4.00	3.50	3.60
				3.60	3.70
				3.70	3.85
				3.85	4.00
				4.00	4.20
				4.20	4.40
				4.40	4.60
				4.60	4.80
				4.80	5.00

$$\frac{\beta_{ext}}{WC} = \sum_{n=0}^{3} a_n \frac{1}{R_e{}^n} \tag{8}$$

$$\omega = \sum_{n=0}^{3} b_n R_e{}^n \tag{9}$$

$$g = \sum_{n=0}^{3} c_n R^n{}_e \tag{10}$$

where the coefficients a_n, b_n, and c_n are determined in a least squares sense with nonlinear regression. A different set of coefficients is obtained for every spectral band and every habit. Through experimentation it was determined that four coefficients for each optical property were sufficient; that is, more than 4 produced only a slight increase in accuracy. The same conclusion was reached by *Fu and Liou* [1993], who used a similar approach to parameterize the optical properties of hexagonal crystals.

[18] The three optical properties were parameterized for three different band schemes: the six bands used by *Fu and Liou* [1993], the 24 bands defined by *Slingo and Schrecker* [1982], and the 56-band scheme of YANG00 which was used in the definition of optical properties for individual ice crystals. These are listed in Table 2. The six- and 24-band schemes would both be appropriate for climate modeling applications, while the 24- and 56-band schemes would be appropriate for remote sensing applications where top-of-atmosphere (TOA) radiances are simulated.

[19] The optical properties are computed using (4), (5), and (6) directly with the 56-band scheme, which is the same as that of YANG00. For the other two band schemes the band average individual crystal single-scattering albedo, asymmetry parameter, and extinction efficiency were computed by weighting all YANG00 values that fell within a band by their proportion of the solar flux within the band. The optical properties were then computed with (4), (5), and (6). The coefficients for all band schemes are available as described later.

[20] Figure 6 shows the parameterized optical properties of the solid column habit for four size distributions and 56 shortwave bands. The optical properties shown cover the range in effective radius and ice water content in the size distributions. Figure 7 illustrates the accuracy of the parameterization, where accuracy is defined as the difference between actual and parameterized optical properties, expressed as a percentage of the actual value for the solid column habit. Differences between the actual (YANG00) and the parameterized optical properties are generally near zero, but differences as large as 5% do occur, particularly at the longer wavelengths. Differences for other habits are similar. The parameterized optical properties for the six spectral band scheme are shown in Figure 8 for solid columns.

[21] The asymmetry parameter is commonly used with the Henyey-Greenstein (HG) function as an approximation of the scattering phase function. The HG function is defined as

$$P_{\mathrm{HG}}(\theta; g) = \frac{1 - g^2}{(1 + g^2 - 2g\cos\theta)^{3/2}} \tag{11}$$

The function represents forward scattering reasonably well, but it does not capture backscattering behavior. The problem can be remedied through the use of the double Henyey-Greenstein function:

$$P_{\mathrm{dHG}}(\theta) = fP_{\mathrm{HG}}(\theta; g_1) + (1 - f)P_{\mathrm{HG}}(\theta; g_2) \tag{12}$$

where g_2 can be assigned a negative value to account for a backscattering peak and f is a positive fraction in the range [0,1] [cf. *Hu et al.*, 2000].

[22] An example of the integrated scattering phase function and the two HG functions is given in Figure 9 for a strong backscattering case in the visible portion of the spectrum. The asymmetry parameter in (11) is used as g_1 in (12). The parameters g_2 and f were found through iteration, where the optimal values are those that minimize the sum of squared differences between the natural log of the true phase function and the natural log of the

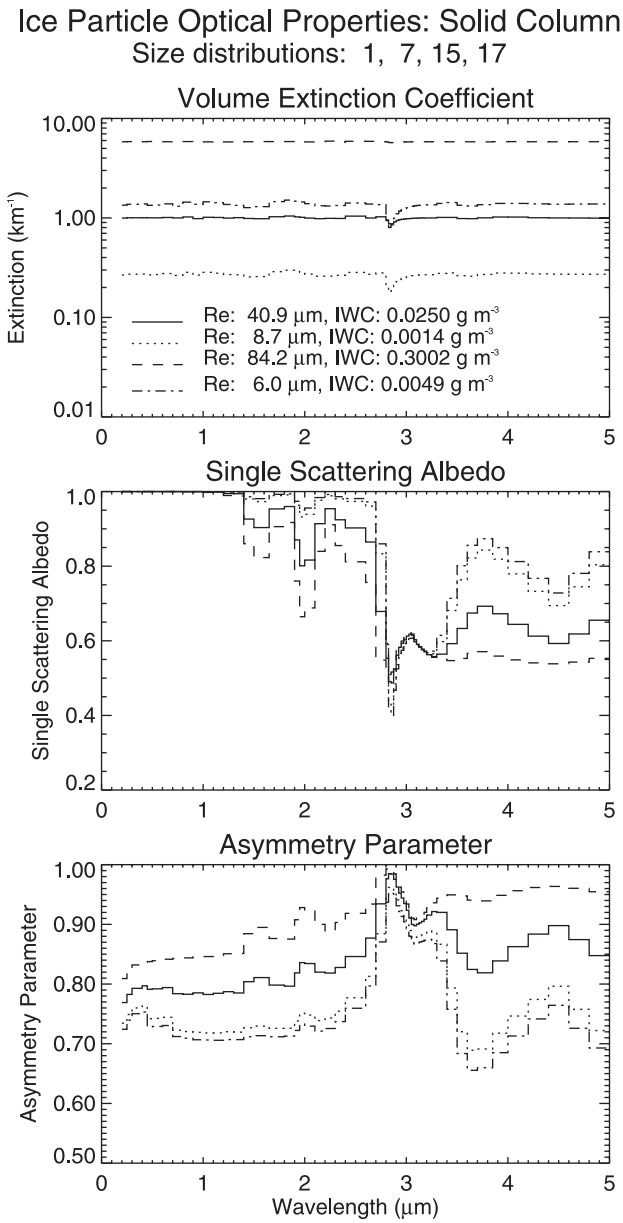

Figure 6. Parameterized optical properties of solid columns for four size distributions and 56 shortwave bands.

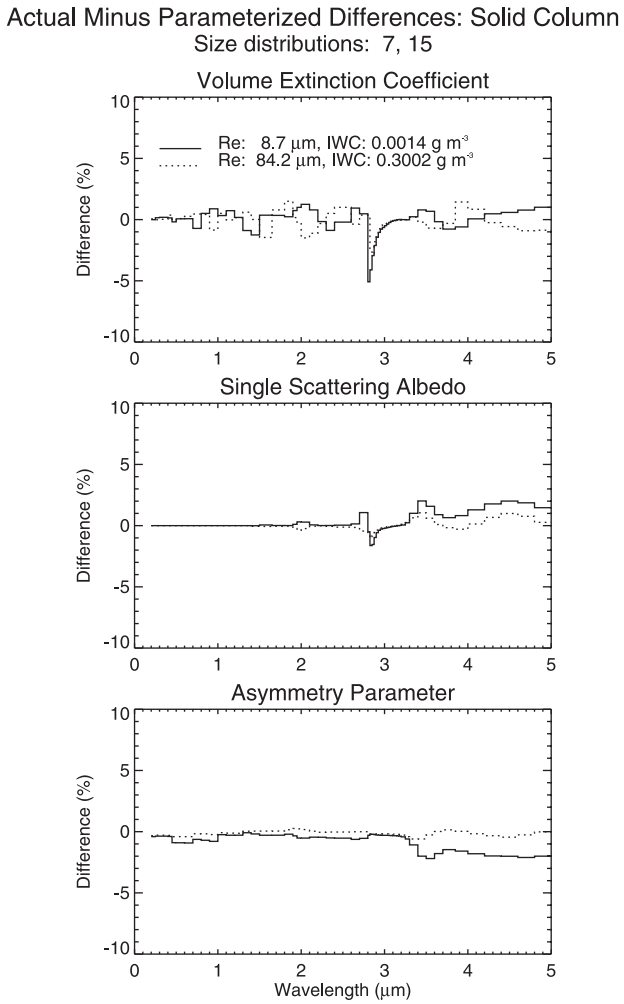

Figure 7. Difference between actual and parameterized optical properties, expressed as a percentage of the actual value (actual minus parameterized divided by actual) for the solid column habit.

double HG function. In this example the value of g_2 is indicative of relatively strong backscattering, so the double HG function better represents the true phase function overall. At the longer wavelengths, g_2 may approach zero and f may be near 1.0, tending toward the single HG function.

[23] Unlike the relationship between g and effective radius (Figure 5), values of g_2 and f for all size distributions exhibited no obvious dependence on particle size. They do, however, vary with wavelength. No parameterization of g_2 and f was therefore attempted. Instead, values for each habit and wavelength are determined.

[24] Validation of the optical properties is a complex task. A far more extensive set of in situ data is needed than is currently available. Measurements of the vertical distribution of particle shape, size, and concentration, with coincident measurements of the cloud bulk radiative properties, are required for a thorough comparison with radiative transfer calculations. In lieu of such a complete set of measurements we compare cloud albedo calculated with the optical properties presented here to that calculated by *Liou et al.* [2000]. In that study, calculations of solar albedo, based on their parameterization of optical properties for hexagonal columns, were compared to observations collected during the First ISCCP Regional Experiment (FIRE) project conducted in Wisconsin during October 1986. The observations covered a range of cloud albedos and water paths [*Liou et al.*, 2000, Figure 11]. They demonstrated that calculations using spherical particles did not give results consistent with the observations, while calculations with hexagonal crystals did. We have duplicated those calculations, taking into account differences in the size definition, and found that our results are consistent with theirs. A more thorough comparison that

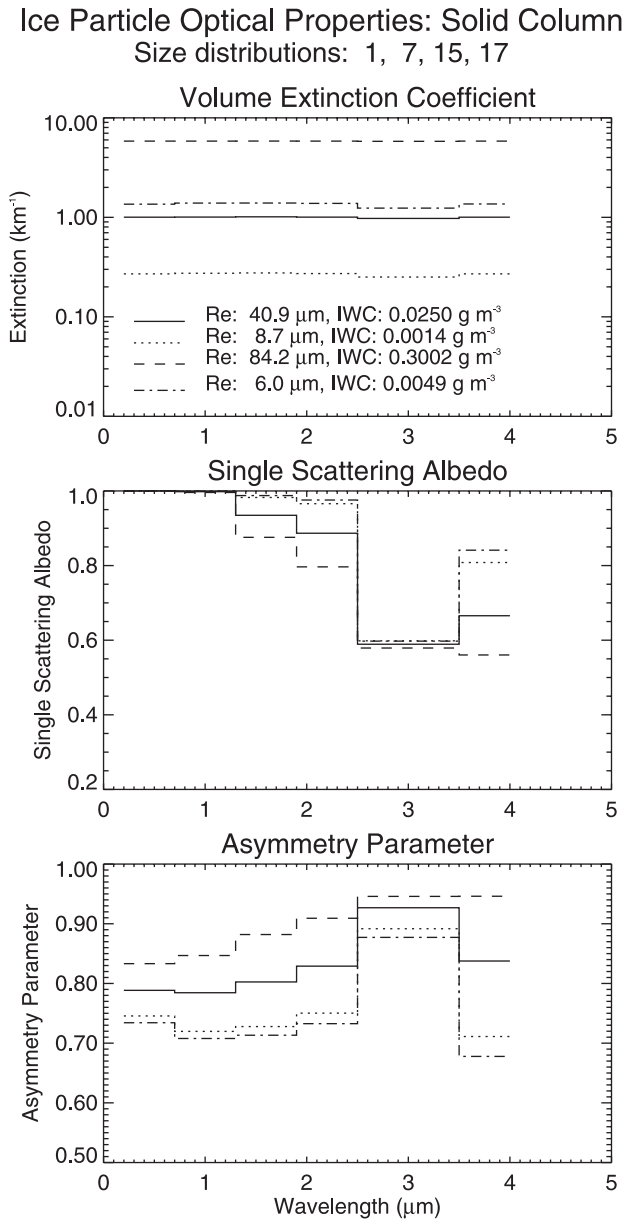

Figure 8. Parameterized optical properties of solid columns for the six-band scheme and for four size distributions.

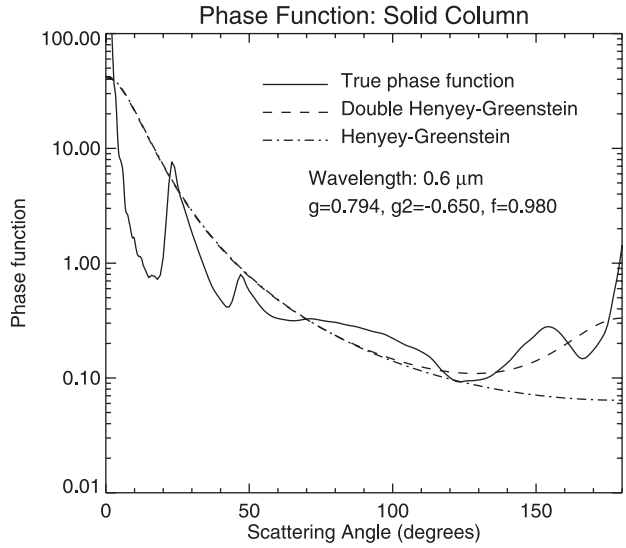

Figure 9. True phase function and the single and double Henyey-Greenstein functions for one size distribution, particle habit, and wavelength. Parameters of the Henyey-Greenstein functions are given. For the double Henyey-Greenstein function, $g_1 = g$.

includes other particle habits cannot be done with existing data sets.

2.4. Mixtures

[25] In nature, ice clouds are often composed of more than one particle habit. It would therefore be useful to parameterize the optical properties of these clouds in a way that includes the fraction of the cloud comprising a particular habit. For example, the volume extinction coefficient could be defined as

$$\beta_{ext} = \sum_{L=L_{min}}^{L_{max}} \sum_{h=1}^{7} f(h,L)\beta_{ext}(h,L)n(L)\Delta L \tag{13}$$

where h represents a particular habit, $f(h, L)$ is the fraction of the total that habit h occupies for the size bin represented by the maximum dimension L. The single-scattering albedo and asymmetry parameter could be computed similarly. However, our knowledge of ice cloud composition is limited in that there is little information available to choose one set of habits and their proportions over another. Therefore a more general solution to combining the optical properties of arbitrary habit combinations is sought at the possible expense of accuracy.

[26] To compute the optical properties of arbitrary particle habit mixtures, we follow the procedure of *Cess* [1985]:

$$\beta_{ext} = \beta_1 + \beta_2 \tag{14}$$

$$\omega = \frac{\omega_1\beta_1 + \omega_2\beta_2}{\beta_1 + \beta_2} \tag{15}$$

$$g = \frac{g_1\omega_1\beta_1 + g_2\omega_2\beta_2}{\omega_1\beta_1 + \omega_2\beta_2} \tag{16}$$

where the subscripts 1 and 2 refer to any two different ice habits. This could easily be extended to mixtures with more than two particle shapes. The g_2 and f parameters of the double Henyey-Greenstein function can be determined for mixtures in the same way as g in (16).

3. Application

[27] In this section the optical properties of the different habits are used to illustrate the effect that particle habit can have on calculations of the downwelling shortwave flux at the surface and in remote sensing applications. In both examples the radiative transfer model Streamer [*Key and Schweiger*, 1998] is used. Streamer uses the 24-band shortwave scheme of *Slingo and Schrecker* [1982], and it utilizes the parameterization described here. The model contains both two-stream and discrete-ordinate solvers. For the downwelling flux example the two-stream method is used. In the remote sensing application the discrete-ordinate radiative transfer solver DISORT [*Stamnes et al.*, 1988] with eight streams is employed. A midlatitude summer atmosphere and a vegetation surface were used in the calculations.

[28] The cloud radiative effect, or cloud "forcing," describes the effect of cloud cover on the net radiation balance. In this example we are only interested in the shortwave cloud forcing, defined as

$$CF_z = \int_0^{A_c} \frac{\partial S_z}{\partial a} da = S_z(A_c) - S_z(0) \tag{17}$$

where S_z is the net shortwave flux (W m^{-2}) at either the surface or the TOA (z), and A_c is the cloud fraction in the scene. The net flux is equal to the downwelling minus the upwelling fluxes. The first term on the right-hand side of the equation is the net flux for all-sky conditions, including clear sky. Figure 10 shows the shortwave cloud

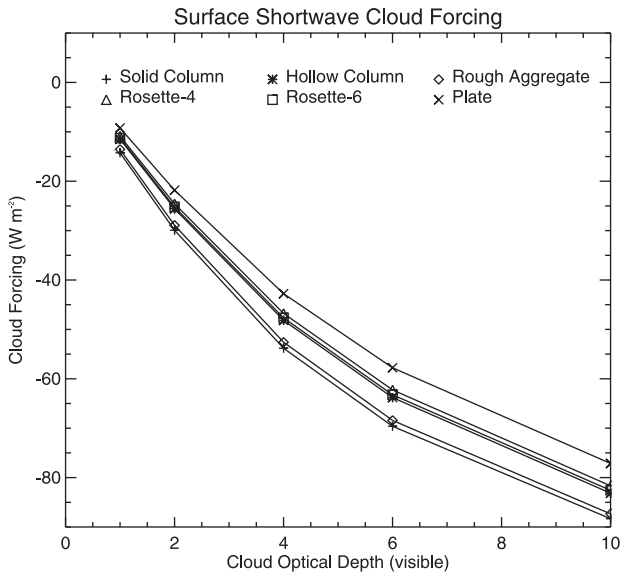

Figure 10. Shortwave cloud radiative effect at the surface for six of the seven habits. Effective radius (20 μm) and water content (0.1 g m^{-3}) are the same for all habits shown. A midlatitude summer atmosphere over a vegetation surface were used in the calculations.

radiative effect at the surface for six of the seven habits. Because the effective radius (20 μm) and ice water content (0.1 g m^{-3}) are the same for all habits shown, differences in cloud forcing are almost exclusively due to particle habit. Cloud thickness, which is a function of the ice water content and the volume extinction coefficient, has a negligible effect. Differences can be large, on the order of 16%, with solid columns and plates comprising opposite extremes of the cloud radiative effect.

[29] The influence of particle habit on TOA radiances can be even more significant than for downwelling surface fluxes. This is primarily due to large differences in the directional scattering, as described by the scattering phase function and the asymmetry parameter. Therefore under certain combinations of illumination and viewing geometries in remote sensing applications, the particle habit assumption is critical. *Yang et al.* [2001] and *Rolland et al.* [2000] showed that the vertical distribution of particle habit affects the near-infrared reflectances calculated from radiative transfer models, which in turn will affect the retrieved particle sizes. In another study, *Baran et al.* [1999] used the dual view geometry (forward and nadir) of the ATSR-2 to estimate the most probable dominating crystal shape at 0.87 μm. Their cirrus models were derived assuming a single crystal habit (hexagonal plates, hexagonal columns, six-branched bullet rosettes, and randomized polycrystals) for each given cirrus size distribution. The reflectances computed from these cirrus scattering models were subsequently compared to selected ATSR-2 data from a tropical convective cirrus case and a midlatitude cirrus case. For the tropical case, the best comparison between the ATSR-2 data at 0.87 μm and radiative transfer calculations was obtained for the randomized polycrystal. One reason for this may be due to the lack of enhanced intensity features in the phase function for polycrystals at backscattering angles. *Francis et al.* [1999] discusses results obtained for a midlatitude cirrus case where a comparison was made between extinction optical depth retrievals using ATSR-2 measured radiances, aircraft measurements of midlatitude cirrus at 0.87 and 11 μm, and in situ calculated optical thicknesses. For their midlatitude cirrus case, *Francis et al.* [1999] found that the best comparison between models and measurements was obtained using a phase function obtained from laboratory measurements [*Volkovitskiy et al.*, 1980] rather than from the randomized polycrystal. Additionally, *Chepfer et al.* [1998, 1999a] have shown the importance of ice crystal habit in the analysis of polarized radiances measured by the POLDER instrument on an aircraft or on the Advanced Earth Observing Satellite-1 (ADEOS-1). The impact of ice crystal shape and size has also been shown to be important for application to spaceborne and airborne backscatter lidar measurements [*Chepfer et al.*, 1999b]. Taken together, these studies indicate that for different applications, the user may require more control over the ability to vary both particle distribution and habit.

[30] Figure 11 shows TOA visible reflectance as a function of cloud optical depth for six different particle habits. As in the previous example, the effective radius (20 μm) and ice water content (0.1 g m^{-3}) are the same for all habits. In the simulation the Henyey-Greenstein function was used to represent the scattering phase function. As before, solid columns and rough aggregates behave similarly and are most dissimilar to the reflectance of plates. The figure illustrates that in an inversion problem, where cloud optical depth is inferred from the visible reflectance, errors can be up to a factor of 2. For example, a visible reflectance of 0.6 implies an optical depth of approximately 10 for a cloud composed of plates but an optical depth of only 4 for solid columns or aggregates.

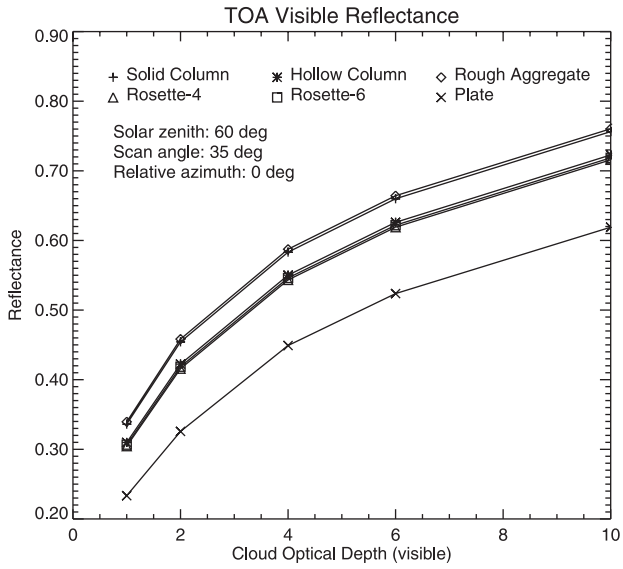

Figure 11. Top-of-atmosphere visible reflectance as a function of cloud optical depth for six different particle habits.

4. Conclusions

[31] The complexity of ice cloud microphysical characteristics and the dearth of in situ measurements of those properties leaves us with many questions about their role in "greenhouse" warming and in the climate system overall. This should not come as a surprise, given the large variability in ice particle size, shape, and density in the atmosphere. To better understand the role of ice clouds in the climate system, parameterizations of their radiative properties are needed. In this paper we have presented parameterizations of the shortwave bulk optical properties for seven ice particle shapes, or "habits." The particle habits are solid and hollow hexagonal columns, hexagonal plates, two- and three-dimensional bullet rosettes, aggregates of columns, and dendrites. The single-scattering albedo and asymmetry parameter were parameterized as a function of the particle effective "radius," which is a function of the particle volume and projected area. The volume extinction coefficient was parameterized as a function of the effective radius and the ice water content. Parameterizations were developed for 6, 24, and 56 band shortwave schemes. Parameterizations of the scattering phase function and longwave optical properties are under investigation.

[32] Validation of the optical properties is a complex task. Measurements of the vertical distribution of particle shape, size, and concentration, with coincident measurements of the cloud bulk radiative properties (e.g., cloud albedo) are required for a useful comparison with radiative transfer calculations employing the optical properties presented

here. A comparison of cloud albedo for one habit with that of *Liou et al.* [2000] indicates that the two methods are consistent and that the new optical properties yield a range of cloud radiative properties consistent with observations. A more extensive validation exercise is the subject of future research.

[33] Applications to downwelling flux and upwelling radiance calculations were presented. Differences of more than 15% in the downwelling shortwave flux were found for clouds with the same effective radius and ice water content but different particle habits. In an example of retrieving cloud optical thickness from visible satellite reflectances, different habits resulted in optical depth differences of more than 50%.

5. Data Availability

[34] Coefficients of the optical property parameterizations for the 6-, 24-, and 56-band schemes are available from the authors. All coefficients are available for download at http://stratus.ssec.wisc.edu. The radiative transfer model Streamer is available at the same location.

[35] **Acknowledgments.** This research was supported by NSF grant OPP-0096085 and NASA grants NAG-1-02002, NAG5-8625, and NAS5-31367. The authors thank Q. Fu for proving the size distribution data, and Don Anderson, NASA Headquarters, for support.

References

Baran, A. J., P. D. Watts, and P. N. Francis, Testing the coherence of cirrus microphysical and bulk properties retrieved from dual-viewing multispectral satellite radiance measurements, *J. Geophys. Res.*, *104*, 31,671–31,683, 1999.

Cess, R. D., Nuclear war: Illustrative effects of atmospheric smoke and dust upon solar radiation, *Clim. Change*, *7*, 237–251, 1985.

Chepfer, H., G. Brogniez, and Y. Fouquart, Cirrus cloud microphysical properties deduced from POLDER observations, *J. Quant. Spectrosc. Radiat. Transfer*, *30*, 375–390, 1998.

Chepfer, H., G. Brogniez, L. Sauvage, P. H. Flamant, V. Trouillet, and J. Pelon, Remote sensing of cirrus radiative parameters during EUCREX'94, Case study of 17 April 1994, part II, Microphysical models, *Mon. Weather Rev.*, *127*, 504–518, 1999a.

Chepfer, H., J. Pelon, G. Brogniez, C. Flamant, V. Trouillet, and P. H. Flamant, Impact of cirrus cloud ice crystal shape and size on multiple scattering effects: Application to spaceborne and airborne backscatter lidar measurements during LITE mission and E LITE campaign, *Geophys. Res. Lett.*, *26*, 2203–2206, 1999b.

Ebert, E. E., and J. A. Curry, A parameterization of ice cloud optical properties for climate models, *J. Geophys. Res.*, *97*(D4), 3831–3836, 1992.

Francis, P. N., J. S. Foot, and A. J. Baran, Aircraft measurements of the solar and infrared radiative properties of cirrus and their dependence on ice crystal shape, *J. Geophys. Res.*, *104*, 31,685–31,695, 1999.

Fu, Q., An accurate parameterization of the solar radiative properties of cirrus clouds for climate models, *J. Clim.*, *9*, 2058–2082, 1996.

Fu, Q., and K. N. Liou, Parameterization of the radiative properties of cirrus clouds, *J. Atmos. Sci.*, *50*(13), 2008–2025, 1993.

Grenfell, T. C., and S. G. Warren, Representation of a nonspherical ice particle by a collection of independent spheres for scattering and absorption of radiation, *J. Geophys. Res.*, *104*, 31,711–31,720, 1999.

Heymsfield, A. J., and C. M. R. Platt, A parameterization of the particle size spectrum of ice clouds in terms of the ambient temperature and the ice water content, *J. Atmos. Sci.*, *41*, 846–855, 1984.

Hu, Y.-X., B. Weilicki, B. Lin, G. Gibson, S.-C. Tsay, K. Stamnes, and T. Wong, Delta-fit: A fast and accurate treatment of particle scattering phase functions with weighted singular-value decomposition least-squares fitting, *J. Quant. Spectrosc. Radiat. Transfer*, *65*, 681–690, 2000.

Iaquinta, J., H. Isaka, and P. Personne, Scattering phase function of bullet rosette ice crystals, *J. Atmos. Sci.*, *52*, 1401–1413, 1995.

Key, J., and A. J. Schweiger, Tools for atmospheric radiative transfer: Streamer and FluxNet, *Comput. Geosci.*, *24*(5), 443–451, 1998.

Liou, K. N., Influence of cirrus clouds on weather and climate processes: A global perspective, *Mon. Weather Rev.*, *114*, 1167–1199, 1986.

Liou, K. N., *Radiation and Cloud Processes in the Atmosphere*, 487 pp., Oxford Univ. Press, New York, 1992.

Liou, K. N., Y. Takano, and P. Yang, Light scattering and radiative transfer in ice crystal clouds: Applications to climate research, in *Light Scattering by Nonspherical Particles: Theory, Measurements and Applications*, 690 pp., edited by M. I. Mishchenko, J. W. Hovenier, and L. D. Travis, Academic, San Diego, 2000.

Macke, A., J. Muller, and E. Raschke, Single scattering properties of atmospheric crystals, *J. Atmos. Sci.*, *53*, 2813–2825, 1996.

Mitchell, D. L., S. K. Chai, Y. Liu, A. J. Heymsfield, and Y. Dong, Modeling cirrus clouds, part I, Treatment of bimodal size spectra and case study analysis, *J. Atmos. Sci.*, *53*, 2952–2966, 1996a.

Mitchell, D. L., A. Macke, and Y. Liu, Modeling cirrus clouds, part II, Treatment of radiative properties, *J. Atmos. Sci.*, *53*, 2967–2987, 1996b.

Rolland, P., K. N. Liou, M. D. King, S. C. Tsay, and G. M. McFarquhar, Remote sensing of optical and microphysical properties of cirrus clouds using Moderate-Resolution Imaging Spectroradiometer channels: Methodology and sensitivity to physical assumptions, *J. Geophys. Res.*, *105*, 11,721–11,738, 2000.

Sassen, K., D. O. Starr, G. G. Mace, M. R. Poellot, S. H. Melfi, W. L. Eberhard, J. D. Spinhire, E. W. Eloranta, D. E. Hagen, and J. Hallett, The 5–6 December 1991 FIRE IFO II jet stream cirrus case study: Possible influences of volcanic aerosols, *J. Atmos. Sci.*, *42*, 97–123, 1995.

Slingo, A., and H. M. Schrecker, On the shortwave radiative properties of stratiform water clouds, *Q. J. R. Meteorol. Soc.*, *108*, 407–426, 1982.

Stamnes, K., S.-C. Tsay, W. Wiscombe, and K. Jayaweera, Numerically stable algorithm for discrete-ordinate-method radiative transfer in multiple scattering and emitting layered media, *Appl. Opt.*, *27*, 2502–2509, 1988.

Stephens, G. L., S.-C. Tsay, P. W. Stackhouse Jr., and P. J. Flatau, The relevance of the microphysical and radiative properties of cirrus clouds to climate and climate feedback, *J. Atmos. Sci.*, *47*, 1742–1753, 1990.

Takano, Y., and K. N. Liou, Solar radiative transfer in cirrus clouds, part I, Single-scattering and optical properties of hexagonal ice crystals, *J. Atmos. Sci.*, *46*, 3–19, 1989.

Takano, Y., and K. N. Liou, Radiative transfer in cirrus clouds, part III, Light scattering by irregular ice crystals, *J. Atmos. Sci.*, *52*, 818–837, 1995.

Volkovitskiy, O. A., L. N. Pavlova, and A. G. Petrushin, Scattering of light by ice crystals, *Atmos. Oceanic Phys.*, *16*, 90–102, 1980.

Wylie, D. P., W. P. Menzel, H. M. Woolf, and K. L. Strabala, Four years of global cirrus cloud statistics using HIRS, *J. Clim.*, *7*, 1972–1986, 1994.

Wyser, K., and P. Yang, Average ice crystal size and bulk short-wave single-scattering properties of cirrus clouds, *Atmos. Res.*, *49*, 315–335, 1998.

Yang, P., and K. N. Liou, Finite-difference time domain method for light scattering by small ice crystals in three-dimensional space, *J. Opt. Soc. Am. Ser. A.*, *13*, 2072–2085, 1996a.

Yang, P., and K. N. Liou, Geometric-optics-integral-equation method for light scattering by nonspherical ice crystals, *Appl. Opt.*, *35*, 6568–6584, 1996b.

Yang, P., and K. N. Liou, Single-scattering properties of complex ice crystals in terrestrial atmosphere, *Contrib. Atmos. Phys.*, *71*, 223–248, 1998.

Yang, P., K. N. Liou, K. Wyser, and D. Mitchell, Parameterization of the scattering and absorption properties of individual ice crystals, *J. Geophys. Res.*, *105*, 4699–4718, 2000.

Yang, P., B. C. Gao, B. A. Baum, W. Wiscombe, Y. Hu, S. L. Nasiri, P. F. Soulen, A. J. Heymsfield, G. M. McFarquhar, and L. M. Miloshevich, Sensitivity of cirrus bidirectional reflectance to vertical inhomogeneity of ice crystal habits and size distributions for two Moderate Resolution Imaging Spectrometer (MODIS) bands, *J. Geophys. Res.*, *106*(D15), 17,267–17,291, 2001.

J. R. Key, Office of Research and Applications, NOAA/NESDIS, 1225 West Dayton Street, Madison, WI 53706, USA. (jkey@ssec.wisc.edu)

P. Yang, Department of Atmospheric Sciences, Texas A&M University, College Station, TX 77843, USA.

B. A. Baum, NASA Langley Research Center, Hampton, VA 23665, USA.

S. L. Nasiri, Cooperative Institute for Meteorological Satellite Studies, University of Wisconsin, Madison, WI 53706, USA.